α-Cellulose-Based Films: Effect of Sodium Lignosulfonate (SLS) Incorporation on Physicochemical and Antibacterial Performance

Xinyu Lu
Nanjing Forestry University
Han Que
Nanjing Forestry University
Haoquan Guo
Nanjing Forestry University
Chenrong Ding
Nanjing Forestry University
Xu Liu
Nanjing Forestry University
Yu Qin
Nanjing Forestry University
Hossain Mahmud Robin
Nanjing Forestry University
Chaozhong Xu
Nanjing Forestry University
Xiaoli GU (guxiaoli@njfu.edu.cn)
Nanjing Forestry University https://orcid.org/0000-0001-8588-0358

Research Article

Keywords: Cellulose, Sodium lignosulfonate, Regeneration, Crosslinking structure

Posted Date: March 11th, 2021

DOI: https://doi.org/10.21203/rs.3.rs-269221/v1

Abstract

A homogeneous *α*-cellulose film was prepared by regeneration method from $ZnCl_2$/$CaCl_2$/cellulose mixed system and was further combined with sodium lignosulfonate (SLS) by crosslinking through interaction hydrogen bonds and “bridge linkages”. The physicochemical and antibacterial performance of films were all investigated and results showed that modified films exhibited stronger tensile strength, higher thermal stability, lower hydrophilic effect, better UV shielding as compared with those of pure cellulose film, and especially, better antibacterial ability derived from the presence of phenolic and sulfonate groups in SLS. This study proposed a simple and sustainable method for fabricating a multifunctional and environmentally friendly composite film by using two main lignocellulose resources as raw materials.

Highlights

- A novel lignin-containing cellulose film was fabricated via crosslinking.
- Superior tensile strength was obtained due to dense crosslinking structure.
- Excellent antibacterial effect was derived from inherent structure of SLS.

1. Introduction

Cellulose, as one of the three main ingredients in lignocellulosic biomass, is a famous biopolymer and has great potential for preparing film-based materials (Khalili et al., 2018; Koli et al., 2018; Zhang et al., 2017). The properties of bio-compatibility, flexibility, chemical modification, and universal applicability make cellulose-based films promising to be utilized in fields of wastewater treating, wound healing, packaging, and bacteriostasis (Hu & Wang, 2016; Kong et al., 2014; Lv et al., 2018; Puspasari et al., 2018; Wang et al., 2019; Wen et al., 2019).

Recently, the regenerated cellulose film derived from regenerated method is a promising alternative to polymeric one (Puspasari et al., 2018). Many works have focused on the investigation of regenerated method due to its excellent bio-compatibility, and nontoxicity (Lee & Jeong, 2015; Pang et al., 2015). For instance, Weng et al. prepared the regenerated cellulose film through phase inversion, where N-methylmorpholine-N-oxide (NMMO) was used as a solvent for dissolving cellulose, and the obtained film exhibited high rejection rate (99.7 %) for Congo red (Weng et al., 2017). Nevertheless, the pure regenerated cellulose film is hydrophilic, poor thermal stability, bacteria prevention, and mechanical properties (Mao et al., 2006; Ruan et al., 2004). Chemical modification or blended with other polymers is effective pathway for addressing this issue through introducing different functional groups and modifying the inherent structure.

Sodium lignosulfonate (SLS) is a by-product produced via the production of wood pulp by using sulfite pulping processes. Approximately 50 million tons of SLS can be obtained every year, where 95 % of this resource is consumed by direct combustion for low-efficiency electricity supply (Kim & Um, 2020; Xu et al., 2020), thus forming a waste of lignin with high efficiency of SLS. Fortunately, abundant presence of

active groups, such as hydroxyl (O-H) and sulfonate ($R\text{-}SO_3^-Na^+$), and various linkages, including C-O and C-C, make SLS reactive for oxidation, reduction, and polymerization reactions. In particular, as a promising alternative of polyol, various types of lignin can crosslink with other aldehydes, polyols, acid anhydrides, and amines for preparing bio-based adhesive (Ang et al., 2019; Chen et al., 2020; Vázquez et al., 1995; Zhang et al., 2013). Recently, lignin-containing cellulose mixed films have obtained broad attention due to their wide distribution, low production cost, and environmental friendliness (Rojo et al., 2015). With the incorporation of lignin, the related properties (e.g., mechanical performance, thermal stability, UV transmission, and hydrophobic effect) of mixed films can be improved significantly (Nair & Yan, 2015; Wen et al., 2019). Therefore, combining lignin and cellulose via crosslinking method is a promising and innovative strategy for preparing lignin-containing cellulose mixed films.

Recently, an inorganic salt system (zinc chloride/calcium chloride) was researched for preparing cellulose films (Xu et al., 2016). Therefore, we prepared regenerated films (including pure and mixed films with different content of SLS) through inorganic co-system ($ZnCl_2/CaCl_2$), and modified these obtained films through crosslinking with assistance of succinic anhydride and triethanolamine. The result showed that the modified mixed film (cellulose/SLS-M) with assistance of succinic anhydride and triethanolamine acting as crosslinking agents exhibited excellent properties (such as thermal stability, hydrophobic effect, mechanical performance, and UV transmission) as compared with those of original one, and the improved performance of bacteriostasis was mainly derived from the addition of SLS.

2. Materials And Methods

2.1. Materials

In this study, *α*-cellulose with particle size of 250 *μ*m used was purchased from Aladdin (Shanghai, China). Sodium lignosulfonate (SLS, 96 %) was purchased from TCI (Shanghai, China), and other chemical reagents, such as zinc chloride ($ZnCl_2$, 99 %), calcium chloride ($CaCl_2$, ≥ 99.9 %), absolute ethanol (≥ 99.5 %), succinic anhydride (98 %), triethanolamine (98 %), anhydrous calcium sulfate ($CaSO_4$, 97 %), sodium carbonate anhydrous (Na_2CO_3, ≥ 99.5 %) were all purchased from Macklin (Shanghai, China). All chemical reagents were utilized without any pretreatment, and deionized water was produced from our lab.

2.2. Preparation of mixed cellulose films

These cellulose films (CFs, including pure and mixed cellulose films which contained different amounts of SLS) were prepared via a regeneration method reported in a previously reported literature (Hou et al., 2019). Typically, 0.45 g *α*-cellulose was added into 1.05 g deionized water to obtain a cellulose suspension liquid. Afterwards, continuous stir was performed in a beaker (10 mL) for 30 min to achieve uniform dispersion of cellulose, which was recorded as solution 1. Then, 9.87 g $ZnCl_2$ and 0.30 g $CaCl_2$ were mixed into 3.63 g deionized water. After 30 min stir, different amounts of SLS (10, 20, 30, and 40 wt% based on the mass of cellulose) were added into this homodisperse metal precursor solution, and

were stirred at 75 ^{o}C for 30 min together, which was named as solution 2. After that, solution 2 was dropwise added into solution 1 with intense stir and was further stirred at room temperature for 12 h to make these two solutions mix well. Finally, the obtained solution was placed under vacuum atmosphere to remove air bubbles and was casted on a glass plate to prepare the film with thickness of 450 μm, and then it was immersed in 450 mL absolute ethanol for 1 h to separate the film from glass plate, which was immediately fixed with two splints and dried at room temperature overnight. The prepared film was tailored with size of 2 cm × 2 cm for the next characterization and was denoted as SLS_x-CF, where x means the mixed addition of SLS (wt%). For instance, SLS_0-CF represents the pure CF without extra addition of SLS, while SLS_{10}-CF means the mixed CF with the addition of 10 wt% SLS.

2.3. Modification process

Due to the presence of hydroxyl groups (O-H) in structures of cellulose and lignin, they have the potential to be utilized as polyols for the achievement of crosslinking (Feng et al., 2021; Lamaming et al., 2020; Yin et al., 2020). Typically, it is difficult to realize mutual crosslinking between two macromolecules through chemical pathways due to their complex structures and unclear reaction mechanism. Therefore, the introduction of “bridge monomers” (succinic anhydride and triethanolamine) is beneficial for improving the interconnection between these two macromolecules. Generally, the polymerization reaction occurs between carboxylic acids and alcohols at a certain temperature to form polymeric esters. In theory, it is feasible to combine cellulose and lignin through this mechanism mentioned above. In this section, succinic anhydride and triethanolamine were utilized as “bridge monomers” (i.e., crosslinking agents) to improve the interconnection between α-cellulose and SLS to form the crosslinking structure, and the specific modification steps are as follow.

First, succinic anhydride (0.18 g), triethanolamine (0.45 g), and different volumes of absolute ethanol (100, 200, and 300 mL) were blended uniformly to prepare organic precursor solutions with different concentrations. Afterwards, the pure CF (i.e., SLS_0-CF) was immersed into different organic precursor solutions for different time (1, 2, and 3 days). Finally, the obtained film after immersion was cured at different temperatures (50, 60, and 70 ^{o}C) for 6 h to make the modification complete. Finally, the film after modification was washed by ethanol for three times to remove unreacted molecules, and dried at curing temperatures (50, 60, and 70 ^{o}C) for 12 h, which was named as CF-M. The performance of obtained films was preliminarily evaluated via their mechanical properties to optimize the modification condition, and results were presented in the next discussion. Other blending films, which contained different amounts of SLS (10, 20, 30, and 40 wt%), were all modified by the optimized condition (300 mL ethanol, 70 ^{o}C curing temperature, and 1 day immersing time), which were assigned as SLS_x-CF-M. During the curing at mild conditions (below 100 ^{o}C), succinic anhydride was hydrolyzed as succinic acid, which can be polymerized with polyols (such as triethanolamine, and hydroxyl groups in structures of cellulose and lignin) to achieve the interconnection of several molecules, and the illustration of modification process is presented in Scheme 1. From the structure displayed in Scheme 1, two internal bonding (interaction

hydrogen bonding and crosslinking derived from “bridge monomers”) can be obtained to fabricate the crosslinking structure of modified blending films.

2.4. Film characterization

The film thickness was measured by an ID-C112XBS micrometer (Mitutoyo Corp., Tokyo, Japan) and presented as average value of five points. FTIR (Fourier transform infrared spectrometer) was performed on a VERTEX 70 spectrometer. The range of measured wavenumbers was between 500–4000 cm^{-1}, and 32 scans per spectrum were collected with a resolution of 4 wavenumbers. The surface morphology was recorded by S-4800 cold field emission SEM (scanning electron microscope). The thermal stability of prepared films was carried out on a TA Instruments TGA (thermo gravimetric analyzer) Q500 (TA Instruments, USA) with a fixed heating rate of 10 ^{o}C/min from room temperature to 600 ^{o}C with nitrogen flow of 40 mL/min. Tensile test was conducted on the film with a strain rate of 30 mm/min at 25 ^{o}C via an auto tensile tester (SANS CMT4000). The film specimens contained width and length of 10 and 35 mm, respectively. The water contact angle was determined by Kruss DSA100. Light transmission was carried out through the film (2 cm × 2 cm) on a Lambda 950 UV-vis spectrometer in the wavelength range of 200–600 cm^{-1}.

The water absorption was measured via Eq. (1):

$$Water\ absorption = \frac{W_t - W_0}{W_0} \times 100\%$$

1

where W_t was the mass of film measured at different immersion time at room temperature after excess surface water was removed.

Water vapor permeance (WVP) was tested by the standard ASTM method E96. Typical bottles with diameter of 2.7 cm and volume of 20 mL were selected to determine the WVP of films. First, the film was cut into a circle with a diameter of 2.8 cm (slight larger than bottle used). After that, a determined amount of anhydrous $CaSO_4$ (RH = 0 %) was added into the bottle until two-thirds volume (approximately 3 g), which was covered by different films. Each bottle was placed into a desiccator (a 100 mL beaker) containing saturated Na_2CO_3 solution at the bottom. Excess amount of Na_2CO_3 was added to ensure the saturability of Na_2CO_3 solution, providing a constant RH of 92 % at 25 ^{o}C. The bottle was weighted every 12 h to record the change of mass, which was recorded as a function of time, and the slope of line (mass change vs. time) was obtained by linear regression. The WVP was determined as the slope divided by the transfer area (g/day m^2).

Antimicrobial activity of films was evaluated by measuring the diameter (cm) of inhibition zone. The bacteria Escherichia coli (*E. coli*) was selected as researching object, which was grown in nutrient broth

liquid medium at 37 ^{o}C for 12 h and further diluted to create a bacteria suspension with the concentration of 1 × 10^{6} CFU (colony forming unit m/L). Diluted bacteria suspension (0.15 mL) of *E. coli* was combined with nutrient agar. Control sample (CF) and modified mixed samples (SLS_{x}-CF-M) were employed to evaluate effects of the presence of SLS on film antimicrobial activity. Films were cut into circle discs at 6 mm in diameter, and further placed on central location of solid agar plates inoculated with testing bacteria *E. coli*, where each solid agar plate was incubated at 37 ^{o}C for 24 h before experiments for the purpose of cleaning zones around the testing film. After experiments, the observed clear zones were places where bacteria growth was inhibited.

All measuring data (e.g., water absorption, WVP, and the diameter of inhibition zone) was recorded in triplicates for each group.

3. Results And Discussion

3.1. FTIR

FTIR spectroscopy is a common characterization for recording the structural change of testing materials, which is presented in Fig. 1. As shown in Fig. 1a, the pure CF exhibits a strong and broad absorbance at around 3300–3350 cm^{-1}, which is assigned to O-H stretching derived from the structure of cellulose. The peak located at 2902 cm^{-1} is attributed to C-H stretching. Other bands for CF mainly appear at 1310, 1102, 102, and 895 cm^{-1}, which are related to the stretching of glucopyranose ring in cellulose (Hu & Wang, 2016). After modification, the peak at 1456 cm^{-1} is due to the presence of C-N originating from triethanolamine, while peaks at □ 1725 and □ 1570 cm^{-1} are characteristic of C = O stretching vibration and carboxylate groups derived from succinic anhydride (Cao et al., 2011; Liu et al., 2009; Sehaqui et al., 2017). Additionally, the peak of CF-M at around 1047 cm^{-1} becomes weaker as compared to that of pure CF, indicating the re-formation of hydrogen bonds caused by the addition of crosslinking agents (Cai et al., 2018). Furthermore, the O-H stretching absorbance of modified film located around 3300–3350 cm^{-1} becomes stronger and shifts to higher wavenumber region, demonstrating the strong intermolecular hydrogen linkage between “bridge monomers” and cellulose, which is a reason for the change of tensile strength (Hu et al., 2016). After being blended with SLS, several changes of functional groups (such as the absorbance of O-H, C-H, and C-O groups) are observed in Fig. 1b. Moreover, the characteristic peak of SLS (i.e., sulfonate group) is located at 615 cm^{-1}, which increases with the increase of SLS content (Liu et al., 2018b).

3.2. SEM

The surface morphology of pure CF, CF-M, and SLS_{x}-CF-M was observed by SEM and shown in Fig. 2. Clearly, the surface of pure CF is homogeneous, while the obvious variation on surface morphology appears after modification to make the film heterogeneous, which is due to the co-existence of different crystalline and amorphous regions derived from different components. With the addition of SLS, the film separation occurs as the content of SLS increases from 10 to

40 wt%, which suggests that CF and SLS become more incompatible. This observation indicates that excess addition of SLS is not beneficial for the effect derived from “bridge monomers” to make the interconnection between cellulose and lignin close, which may be the cause of variation in mechanical property.

3.3. TGA

Figure 3 shows thermosgrams of pure CF and other modified blending films. As presented in Fig. 3, the thermal degradation process is mainly divided into three stages, including moisture evaporation (stage 1, below 150 ^{o}C), rapid decomposition (stage 2, from 150–500 ^{o}C), and carbonization (stage 3, above 500 ^{o}C) stages (Lu et al., 2021). The main decomposition process occurs at stage 2, where the mass loss is mainly attributed to the thermal decomposition of “bridge linking” bonds (e.g., C-O, C = O), cellulose backbone, and lignin structure to form H_2O, CO_2, CH_4, CO, and various aromatic volatiles (de Oliveira Junior et al., 2012; Lu et al., 2020; Mazarin de Moraes et al., 2015). At the stage of carbonization, char formation (around 35 wt%) is inevitable because of the dominant proportion of carbon (C) in lignocellulosic biomass (Laouge & Merdun, 2020; Yeo et al., 2019). In addition, almost no difference is observed during the first stage, while the maximum degradation temperature increases from 304 ^{o}C for pure CF to 305 ^{o}C for SLS_{10}-CF-M, 308 ^{o}C for SLS_{20}-CF-M, 307 ^{o}C for SLS_{30}-CF-M, and 310 ^{o}C for SLS_{40}-CF-M, respectively. The increasing variation can be attributed by the crosslinking effect derived from “bridge monomers”, the interaction hydrogen bonding between cellulose and lignin, or the deterioration of heat and mass transfer in samples after the addition of lignin (Ma et al., 2015). Moreover, several previous studies had reported that the incorporation of lignin (a three-dimensional structure macromolecule) as a natural carbon resource could improve the thermal stability of raw substrate, especially for the field of flame retardant (Dai et al., 2020; Ferdosian et al., 2016; Podkoscielna et al., 2020). Furthermore, not only the improvement of thermal stability during main decomposition process can be achieved, but also the content of condensed phase obtained after pyrolysis also increases, which is caused by structural collapse of cellulose backbone and lignin aromatic units to form the thermostable char with higher crosslinking density. TGA results illustrate that the thermal stability of pure CF is improved obviously, and predictable reasons are as follows: 1) abundant polar bonds (hydroxyls) were introduced with the addition of lignin, which could interact with cellulose via interaction hydrogen bonds to form crosslinking network; 2) the introduction of “bridge monomers” was beneficial to form the interconnection between lignin and cellulose via “bridge linking” bonds (the polymerization of carboxylic acid and alcoholic hydroxyl), thus strengthening the stability of mixed system; 3) three-dimensional structure of lignin was more stable as compared with cellulose, which was harder to be decomposed at high temperatures, as more stable condensed phase (char) with higher thermal stability was generated due to the repolymerization caused by the instability of active functional groups and the regeneration of carbon-carbon bonds.

3.4. Mechanical properties

Table 1
Tensile strength of CF-M prepared via different conditions.

No.	Ethanol/mL	Temperature/^{o}C	Time/day	Tensile strength/MPa
1	a	a	a	56.6
2	a	b	b	46.6
3	a	c	c	47.9
4	b	b	a	56.7
5	b	c	b	60.8
6	b	a	c	56.4
7	c	c	a	64.6
8	c	a	b	50.7
9	c	b	c	55.0
[a] Ethanol: 100 mL; Immersion time: 1 day; Curing temperature: 50 ^{o}C.				
[b] Ethanol: 200 mL; Immersion time: 2 days; Curing temperature: 60 ^{o}C.				
[c] Ethanol: 300 mL; Immersion time: 3 days; Curing temperature: 70 ^{o}C.				

For obtaining the optimized condition of modification in Sect. 2.3, orthogonal experiments for testing tensile strength were performed with three variables (i.e., ethanol volume/mL, immersing time/day, and curing temperature/^{o}C), and each tensile strength presented in Table 1 was the average of three records. From Table 1, the tensile strength of 64.6 MPa was obtained in 300 mL ethanol at 70 ^{o}C for 1 day. More ethanol and less immersion time are beneficial for the film regeneration and maintaining the integrity of obtained films, respectively. Excessing immersing time may slightly destroy the interaction bonding, thus declining the degree of crosslinking (Hu & Wang, 2016). Similarly, higher temperatures will accelerate the crosslinking to strengthen the internal interconnection.

In addition, all films exhibit high tensile strength and relevant strain-to-failure values (see Fig. 4). The pure CF shows a tensile strength of 55.1 MPa and a strain-to-failure value of 18.5 %. After modification, these two values all increase significantly to 66.7 MPa and 20.8 %, respectively, which demonstrates that strong crosslinking bonds are formed after “bridge monomers” addition to extremely improve the mechanical properties. With the incorporation of 10 wt% SLS, the value of tensile strength rises obviously to 67.8 MPa, while that of strain-to-failure declines to 10.6 %. Further increasing SLS addition, both tensile strength and strain-to-failure value all dropped rapidly, which indicated that the strong interaction hydrogen bonding is created between SLS and cellulose film, as proven in FTIR, but phase separation is subsequently formed (see SEM images in Fig. 2), breaking the compatibility of blending system, thus leading to the degradation of mechanical properties. As for SLS_{10}-CF-M, the tensile strength (67.8 MPa) is

higher than that of other reported mixed cellulose films, such as glutaraldehyde-polyvinyl alcohol/cellulose film (5 wt% P-G/RC, 66.3 MPa) (Hou et al., 2019), 5 wt% nanofibrillated cellulose (NFC)/poly(vinyl alcohol) (PVA) film (44.3 MPa) (Xiao et al., 2016), 32 wt% α-cellulose nanofibers (CHFs)/PVA film (39.0 MPa) (Cai et al., 2016).

3.5. Contact angle and water absorption capacity

Figure 5 shows the surface contact angle of different samples, which demonstrates hydrophilic and hydrophobic properties of testing materials, therefore exhibiting water adsorption capacity (see Fig. 6, the average amounts of water absorption of pure CF, SLS_{10-40}-CFs-M are 66.18, 46.73, 57.44, 56.58, and 64.01 %, respectively). All contact angles are less than 90 ^{o}, indicating that all samples are hydrophilic (Wang et al., 2019). However, with the incorporation of SLS, the contact angle of mixed films increases by 10–30 ^{o}, where the highest value of contact angle is obtained at 10 wt% SLS addition. Generally, there are abundant hydrophilic groups in the internal structure of SLS, such as hydroxyl and sulfonate groups. Nevertheless, the worse hydrophilic capacity of mixed films is obtained after SLS addition, and the main reason is that hydroxyl groups in both SLS and cellulose can be interacted with each other to form crosslinking structure. In addition, the formation of “bridge linking” is positive for the decrease of hydroxyl groups, thus lowering hydrophilic ability (Llorens et al., 2015). The excess addition of SLS is negative for the blending film to obtain a compatible system as separation phase (SLS region) is formed on the surface of film, therefore increasing their hydrophilic capacity.

3.6. Light transmittance

The UV transmission of pure CF and modified mixed films was recorded in the range of 200–600 nm, and their transmission curves are shown in Fig. 7. The transmission of pure CF reaches 69.6 % at 280 nm, while that of SLS_{10}-CF-M is 1.2 %, which almost appears opaque. Further increasing the SLS addition from 10 to 40 wt% significantly decreases the transmission of blending films, almost close to 0 %, showing excellent UV blocking performance. These observations suggest that the extra addition of SLS makes the film surface bumpy (see SEM images), thereby inducing optical scattering and refraction. Therefore, with assistance of “bridge linking” and interaction hydrogen bonding, the presence of SLS plays an important role in blocking UV transmission, which make the blending films potential in UV-shielding application.

3.7. *Water vapor permeance (WVP)*

Table 2
Water vapor permeance (WVP) of different samples.

Sample	WVP (g/day m^2)
CF	104.12 ± 20.46
SLS_{10}-CF-M	56.49 ± 15.32
SLS_{20}-CF-M	65.96 ± 12.61
SLS_{30}-CF-M	68.54 ± 17.56
SLS_{40}-CF-M	83.79 ± 15.38

The water vapor permeance (WVP) of different samples is shown in **Table 2**. The pure film exhibits the highest WVP (104.12 g/day m^2). With the addition of SLS (10 wt%), the WVP of blending film decreases significantly from 104.12 to 56.49 g/day m^2, which may be due to the crosslinking effect from “bridge linking” and intense interaction hydrogen bonding between lignin and cellulose to decrease the inter-chain space, thus declining diffusivity and solubility of water molecules, which is corresponding to the result obtained from water absorption and contact angle. However, the hydrophilic property of all films (the contact angles are all less than 90 ^{o}) give them appropriate values of WVP, which are much higher than that of other cellulosic composite films (El Miri et al., 2015; Karkhanis et al., 2018; Liu et al., 2018). With the increase of SLS addition (from 10 to 40 wt%), the WVP of composite films increases from 56.49 to 83.79 g/day m^2. Excess amount of SLS results in phase separation in the film surface, thus making the gap between molecules larger to accelerate the diffusion of water molecules.

3.8. Antibacterial property

The antibacterial ability of different samples was evaluated via measuring the diameter (mm) of inhibition zones, a classic method, which adopted film samples on the central location of agar medium coated with bacteria, and observed the inhibition of growth and propagation of bacteria (*E. coli*) to form a blank circle region around the samples, which was generally named as inhibition zone. According to the result in Fig. 8, the original CF presented as a control sample almost exhibits no inhibition zone against *E. coli*, while an apparent inhibition zone is observed after 10 wt% SLS addition in Fig. 8b, indicating the important role of SLS on antibacterial performance. Increasing the addition of SLS from 10 to 40 wt%, the obtained inhibition zone becomes larger and larger (from 8.0 mm for SLS_{10}-CF-M to 11.0 mm for SLS_{40}-CF-M), which demonstrates that the presence of SLS is beneficial for inhibiting the growth of testing bacteria. Generally, lignin (from hardwood or softwood) contains abundant phenolic hydroxyl groups, which are effective for inhibiting oxidation and bacteria growth (such as *P. aeruginosa*, *S. enteritidis*, *E. coli*, *B. cereus*, *S. aureus*) (Lourencon et al., 2021; Wang et al., 2021). In addition, the special presence of

sulfonate group in SLS as compared with other lignin is also an effectively antibacterial factor (Asadullah et al., 2020).

4. Conclusions

In this study, SLS_X-CF-M composite films were fabricated, and FTIR result demonstrated the completion of blending film preparation. The crosslinking structure formed by interaction hydrogen bonds and “bridge linkages”, and separation phase induced by the increasing addition of SLS were two main reasons for the change of mechanical and hydrophobic properties, while the UV transmission and antibacterial performance were all influenced by the addition of SLS. Treating SLS as a renewable alternative resource of other synthetic polyols or bacteriostatic agent for film modification meets the requirement of sustainable development

Declarations

Acknowledgement

This research was financially supported from the National Natural Science Foundation of China (no.21774059), the Priority Academic Program Development (PAPD) of Jiangsu Higher Education Institutions, the opening funding of Jiangsu Key Lab of Biomass based Green Fuels and Chemicals.

Conflicts of interest/Competing interests

The authors declare that they have no known competing financial interests or personal relationships that could have appeared to influence the work reported in this paper.

References

1. Ang AF, Ashaari Z, Lee SH, Md Tahir P, Halis R 2019 Lignin-based copolymer adhesives for composite wood panels-A review. Int J Adhes Adhes 95:102408. http://doi.org/10.1016/j.ijadhadh.2019.102408.
2. Asadullah S, Mei S, Wang D, Yao Y, Pan Y, Wang D, Guo H, Wei J 2020 Sulfonated porous surface of tantalum pentoxide/polyimide composite with micro-submicro structures displaying antibacterial performances and stimulating cell responses. Mater Design 190:108510. http://doi.org/10.1016/j.matdes.2020.108510.
3. Cai J, Chen J, Zhang Q, Lei M, He J, Xiao A, Ma C, Li S, Xiong H 2016 Well-aligned cellulose nanofiber-reinforced polyvinyl alcohol composite film: Mechanical and optical properties. Carbohyd Polym 140:238-245. http://doi.org/10.1016/j.carbpol.2015.12.039.
4. Cai Q, Fan Z, Chen J, Guo W, Ma F, Sun S, Hu L, Zhou Q 2018 Dissolving process of bamboo powder analyzed by FT-IR spectroscopy. J Mol Struct 1171:639-643. http://doi.org/10.1016/j.molstruc.2018.06.066.

5. Cao W, Dang Z, Zhou XQ, Yi XY, Wu PX, Zhu NW, Lu GN 2011 Removal of sulphate from aqueous solution using modified rice straw: Preparation, characterization and adsorption performance. Carbohyd Polym 85:571-577. http://doi.org/10.1016/j.carbpol.2011.03.016.
6. Chen Y, Zhang H, Zhu Z, Fu S 2020 High-value utilization of hydroxymethylated lignin in polyurethane adhesives. Int J Biol Macromol 152:775-785. http://doi.org/10.1016/j.ijbiomac.2020.02.321.
7. Dai P, Liang M, Ma X, Luo Y, He M, Gu X, Gu Q, Hussain I, Luo Z 2020 Highly Efficient, Environmentally Friendly Lignin-Based Flame Retardant Used in Epoxy Resin. ACS Omega 5:32084-32093. http://doi.org/10.1021/acsomega.0c05146.
8. de Oliveira Junior AR, Favaro Ferrarezi MM, Pagotto Yoshida IV, Goncalves MdC 2012 Cellulose Acetate/Polysilsesquioxane Composites: Thermal Properties and Morphological Characterization by Electron Spectroscopy Imaging. J Appl Polym Sci 123:2027-2035. http://doi.org/10.1002/app.34707.
9. El Miri N, Abdelouahdi K, Barakat A, Zahouily M, Fihri A, Solhy A, El Achaby M 2015 Bio-nanocomposite films reinforced with cellulose nanocrystals: Rheology of film-forming solutions, transparency, water vapor barrier and tensile properties of films. Carbohyd Polym 129:156-167. http://doi.org/10.1016/j.carbpol.2015.04.051.
10. Feng S, Shui T, Wang H, Ai X, Kuboki T, Xu CC 2021 Properties of phenolic adhesives formulated with activated organosolv lignin derived from cornstalk. Ind Crop Prod 161:113225. https://doi.org/10.1016/j.indcrop.2020.113225.
11. Ferdosian F, Yuan Z, Anderson M, Xu CC 2016 Thermal performance and thermal decomposition kinetics of lignin-based epoxy resins. J Anal Appl Pyrol 119:124-132. http://doi.org/10.1016/j.jaap.2016.03.009.
12. Hou T, Guo K, Wang Z, Zhang XF, Feng Y, He M, Yao J 2019 Glutaraldehyde and polyvinyl alcohol crosslinked cellulose membranes for efficient methyl orange and Congo red removal. Cellulose 26:5065-5074. http://doi.org/10.1007/s10570-019-02433-w.
13. Hu D, Wang H, Wang L 2016 Physical properties and antibacterial activity of quaternized chitosan/carboxymethyl cellulose blend films. LWT-Food Sci Technol 65:398-405. http://doi.org/10.1016/j.lwt.2015.08.033.
14. Hu D, Wang L 2016 Preparation and characterization of antibacterial films based on polyvinyl alcohol/quaternized cellulose. React Funct Polym 101:90-98. http://doi.org/10.1016/j.reactfunctpolym.2016.02.012.
15. Karkhanis SS, Stark NM, Sabo RC, Matuana LM 2018 Water vapor and oxygen barrier properties of extrusion-blown poly(lactic acid)/cellulose nanocrystals nanocomposite films. Compos Part A-Appl S 114:204-211. http://doi.org/10.1016/j.compositesa.2018.08.025.
16. Khalili MS, Zare K, Moradi O, Sillanpaa M 2018 Preparation and characterization of MWCNT-COOH-cellulose-MgO NP nanocomposite as adsorbent for removal of methylene blue from aqueous

solutions: isotherm, thermodynamic and kinetic studies. J Nanostructure Chem 8:103-121. http://doi.org/10.1007/s40097-018-0258-5.

17. Kim GH, Um BH 2020 Fractionation and characterization of lignins from Miscanthus via organosolv and soda pulping for biorefinery applications. Int J Biol Macromol 158:443-451. http://doi.org/10.1016/j.ijbiomac.2020.04.229.
18. Koli PB, Kapadnis KH, Deshpande UG, Patil MR 2018 Fabrication and characterization of pure and modified Co_3O_4 nanocatalyst and their application for photocatalytic degradation of eosine blue dye: a comparative study. J Nanostructure Chem 8:453-463. http://doi.org/10.1007/s40097-018-0287-0.
19. Kong L, Zhang D, Shao Z, Han B, Lv Y, Gao K, Peng X 2014 Superior effect of TEMPO-oxidized cellulose nanofibrils (TOCNs) on the performance of cellulose triacetate (CTA) ultrafiltration membrane. Desalination 332:117-125. http://doi.org/10.1016/j.desal.2013.11.005.
20. Lamaming J, Heng NB, Owodunni AA, Lamaming SZ, Abd Khadir NK, Hashim R, Sulaiman O, Kassim MHM, Hussin MH, Bustami Y, Amini MHM, Hiziroglu S 2020 Characterization of rubberwood particleboard made using carboxymethyl starch mixed with polyvinyl alcohol as adhesive. Compos Part B-Eng 183:107731. http://doi.org/10.1016/j.compositesb.2019.107731.
21. Laouge ZB, Merdun H 2020 Pyrolysis and combustion kinetics of Sida cordifolia L. using thermogravimetric analysis. Bioresource Technol 299:122602. http://doi.org/10.1016/j.biortech.2019.122602.
22. Lee TW, Jeong YG 2015 Regenerated cellulose/multiwalled carbon nanotube composite films with efficient electric heating performance. Carbohyd Polym 133:456-463. http://doi.org/10.1016/j.carbpol.2015.06.053.
23. Liu CF, Zhang AP, Li WY, Yue FX, Sun RC 2009 Homogeneous Modification of Cellulose in Ionic Liquid with Succinic Anhydride Using N-Bromosuccinimide as a Catalyst. J Agr Food Chem 57:1814-1820. http://doi.org/10.1021/jf803097k.
24. Liu H, Liu C, Peng S, Pan B, Lu C 2018 Effect of polyethyleneimine modified graphene on the mechanical and water vapor barrier properties of methyl cellulose composite films. Carbohyd Polym 182:52-60. http://doi.org/10.1016/j.carbpol.2017.11.008.
25. Liu X, Song P, Wang B, Wu Y, Jiang Y, Xu F, Zhang X 2018 Lignosulfonate-Directed Synthesis of Consubstantial Yolk-Shell Carbon Microspheres with Pollen-Like Surface from Sugar Biomass. ACS Sustain Chem Eng 6:16315-16322. http://doi.org/10.1021/acssuschemeng.8b03246.
26. Llorens E, Calderon S, del Valle LJ, Puiggali J 2015 Polybiguanide (PHMB) loaded in PLA scaffolds displaying high hydrophobic, biocompatibility and antibacterial properties. Mat Sci Eng C-Mater 50:74-84. http://doi.org/10.1016/j.msec.2015.01.100.
27. Lourencon TV, de Lima GG, Ribeiro CSP, Hansel FA, Maciel GM, da Silva K, Winnischofer SMB, de Muniz GIB, Magalhaes WLE 2021 Antioxidant, antibacterial and antitumoural activities of kraft lignin from hardwood fractionated by acid precipitation. Int J Biol Macromol 166:1535-1542. http://doi.org/10.1016/j.ijbiomac.2020.11.033.

28. Lu X, Guo H, Que H, Wang D, Liang D, He T, Robin HM, Xu C, Zhang X, Gu X 2021 Pyrolysis mechanism and kinetics of high-performance modified lignin-based epoxy resins. J Anal Appl Pyrol 154:105013. http://doi.org/10.1016/j.jaap.2020.105013.
29. Lu X, Zhu X, Guo H, Que H, Wang D, Liang D, He T, Hu C, Xu C, Gu X 2020 Investigation on the thermal degradation behavior of enzymatic hydrolysis lignin with or without steam explosion treatment characterized by TG-FTIR and Py-GC/MS. Biomass Convers Bior http://doi.org/10.1007/s13399-020-00987-5.
30. Lv Y, Du Y, Chen ZX, Qiu WZ, Xu ZK 2018 Nanocomposite membranes of polydopamine/electropositive nanoparticles/polyethyleneimine for nanofiltration. J Membrane Sci 545:99-106. http://doi.org/10.1016/j.memsci.2017.09.066.
31. Ma Z, Chen D, Gu J, Bao B, Zhang Q 2015 Determination of pyrolysis characteristics and kinetics of palm kernel shell using TGA-FTIR and model-free integral methods. Energ Convers Manage 89:251-259. http://doi.org/10.1016/j.enconman.2014.09.074.
32. Mao Y, Zhou J, Cai J, Zhang L 2006 Effects of coagulants on porous structure of membranes prepared from cellulose in NaOH/urea aqueous solution. J Membrane Sci 279:246-255. http://doi.org/10.1016/j.memsci.2005.07.048.
33. Mazarin de Moraes AC, Andrade PF, de Faria AF, Simoes MB, Carneiro Soares Salomao FC, Barros EB, Goncalves MdC, Alves OL 2015 Fabrication of transparent and ultraviolet shielding composite films based on graphene oxide and cellulose acetate. Carbohyd Polym 123:217-227. http://doi.org/10.1016/j.carbpol.2015.01.034.
34. Nair SS, Yan N 2015 Effect of high residual lignin on the thermal stability of nanofibrils and its enhanced mechanical performance in aqueous environments. Cellulose 22:3137-3150. http://doi.org/10.1007/s10570-015-0737-5.
35. Pang J, Wu M, Zhang Q, Tan X, Xu F, Zhang X, Sun R 2015 Comparison of physical properties of regenerated cellulose films fabricated with different cellulose feedstocks in ionic liquid. Carbohyd Polym 121:71-78. http://doi.org/10.1016/j.carbpol.2014.11.067.
36. Podkoscielna B, Wnuczek K, Goliszek M, Klepka T, Dziuba K 2020 Flammability Tests and Investigations of Properties of Lignin-Containing Polymer Composites Based on Acrylates. Molecules 25:5947. http://doi.org/10.3390/molecules25245947.
37. Puspasari T, Huang T, Sutisna B, Peinemann KV 2018 Cellulose-polyethyleneimine blend membranes with anomalous nanofiltration performance. J Membrane Sci 564:97-105. http://doi.org/10.1016/j.memsci.2018.07.002.
38. Rojo E, Peresin MS, Sampson WW, Hoeger IC, Vartiainen J, Laine J, Rojas OJ 2015 Comprehensive elucidation of the effect of residual lignin on the physical, barrier, mechanical and surface properties of nanocellulose films. Green Chem 17:1853-1866. http://doi.org/10.1039/c4gc02398f.
39. Ruan D, Zhang L, Mao Y, Zeng M, Li X 2004 Microporous membranes prepared from cellulose in NaOH/thiourea aqueous solution. J Membrane Sci 241:265-274. http://doi.org/10.1016/j.memsci.2004.05.019.

40. Sehaqui H, Kulasinski K, Pfenninger N, Zimmermann T, Tingaut P 2017 Highly Carboxylated Cellulose Nanofibers via Succinic Anhydride Esterification of Wheat Fibers and Facile Mechanical Disintegration. Biomacromolecules 18:242-248. http://doi.org/10.1021/acs.biomac.6b01548.
41. Vázquez G, Antorrena G, González J, Mayor J 1995 Lignin-phenol-formaldehyde adhesives for exterior grade plywoods. Bioresource Technol 51:187-192. http://doi.org/10.1016/0960-8524(94)00120-P.
42. Wang Y, Li Z, Yang D, Qiu X, Xie Y, Zhang X 2021 Microwave-mediated fabrication of silver nanoparticles incorporated lignin-based composites with enhanced antibacterial activity via electrostatic capture effect. J Colloid Interf Sci 583:80-88. https://doi.org/10.1016/j.jcis.2020.09.027.
43. Wang Y, Wang C, Xie Y, Yang Y, Zheng Y, Meng H, He W, Qiao K 2019 Highly transparent, highly flexible composite membrane with multiple antimicrobial effects used for promoting wound healing. Carbohyd Polym 222:114985. http://doi.org/10.1016/j.carbpol.2019.114985.
44. Wen Y, Yuan Z, Liu X, Qu J, Yang S, Wang A, Wang C, Wei B, Xu J, Ni Y 2019 Preparation and Characterization of Lignin-Containing Cellulose Nanofibril from Poplar High-Yield Pulp via TEMPO-Mediated Oxidation and Homogenization. ACS Sustain Chem Eng 7:6131-6139. http://doi.org/10.1021/acssuschemeng.8b06355.
45. Weng R, Chen L, Xiao H, Huang F, Lin S, Cao S, Huang L 2017 Preparation and Characterization of Cellulose Nanofiltration Membrane Through Hydrolysis Followed by Carboxymethylation. Fiber Polym 18:1235-1242. http://doi.org/10.1007/s12221-017-7200-1.
46. Xiao S, Gao R, Gao L, Li J 2016 Poly(vinyl alcohol) films reinforced with nanofibrillated cellulose (NFC) isolated from corn husk by high intensity ultrasonication. Carbohyd Polym 136:1027-1034. http://doi.org/10.1016/j.carbpol.2015.09.115.
47. Xu J, Li M, Yang L, Qiu J, Chen Q, Zhang X, Feng Y, Yao J 2020 Synergy of Ni dopant and oxygen vacancies in ZnO for efficient photocatalytic depolymerization of sodium lignosulfonate. Chem Eng J 394:125050. https://doi.org/10.1016/j.cej.2020.125050.
48. Xu Q, Chen C, Rosswurm K, Yao T, Janaswamy S 2016 A facile route to prepare cellulose-based films. Carbohyd Polym 149:274-281. http://doi.org/10.1016/j.carbpol.2016.04.114.
49. Yeo JY, Chin BLF, Tan JK, Loh YS 2019 Comparative studies on the pyrolysis of cellulose, hemicellulose, and lignin based on combined kinetics. J Energy Inst 92:27-37. http://doi.org/10.1016/j.joei.2017.12.003.
50. Yin H, Zheng P, Zhang E, Rao J, Lin Q, Fan M, Zhu Z, Zeng Q, Chen N 2020 Improved wet shear strength in eco-friendly starch-cellulosic adhesives for woody composites. Carbohyd Polym 250:116884. http://doi.org/10.1016/j.carbpol.2020.116884.
51. Zhang W, Ma Y, Xu Y, Wang C, Chu F 2013 Lignocellulosic ethanol residue-based lignin-phenol-formaldehyde resin adhesive. Int J Adhes Adhes 40:11-18. http://doi.org/10.1016/j.ijadhadh.2012.08.004.
52. Zhang XF, Feng Y, Huang C, Pan Y, Yao J 2017 Temperature-induced formation of cellulose nanofiber [redacted]n performance. Cellulose 24:5649-5656.

http://doi.org/10.1007/s10570-017-1529-x.

Figures

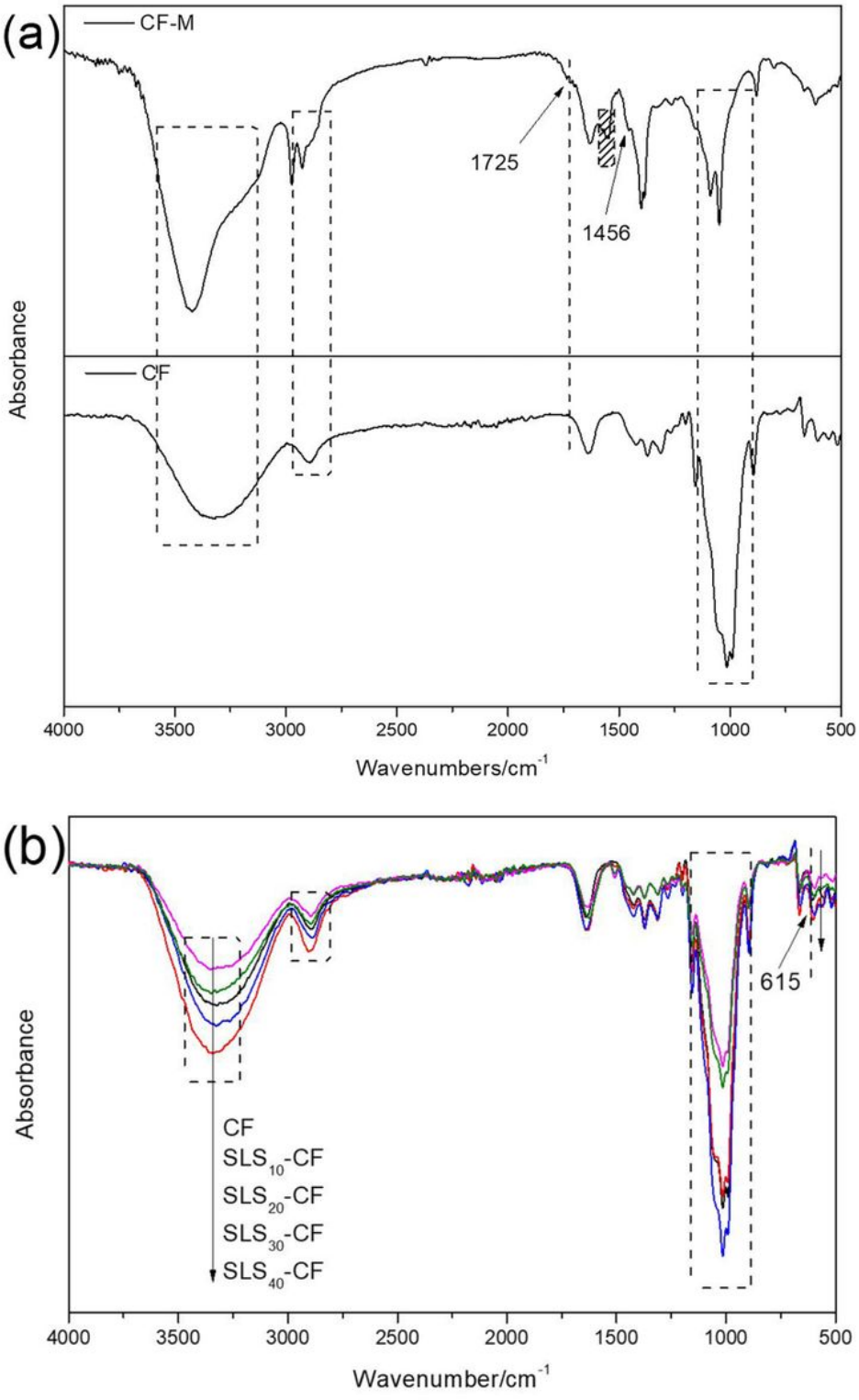

Figure 1

Loading [MathJax]/jax/output/CommonHTML/jax.js ms (SLSx-CF).

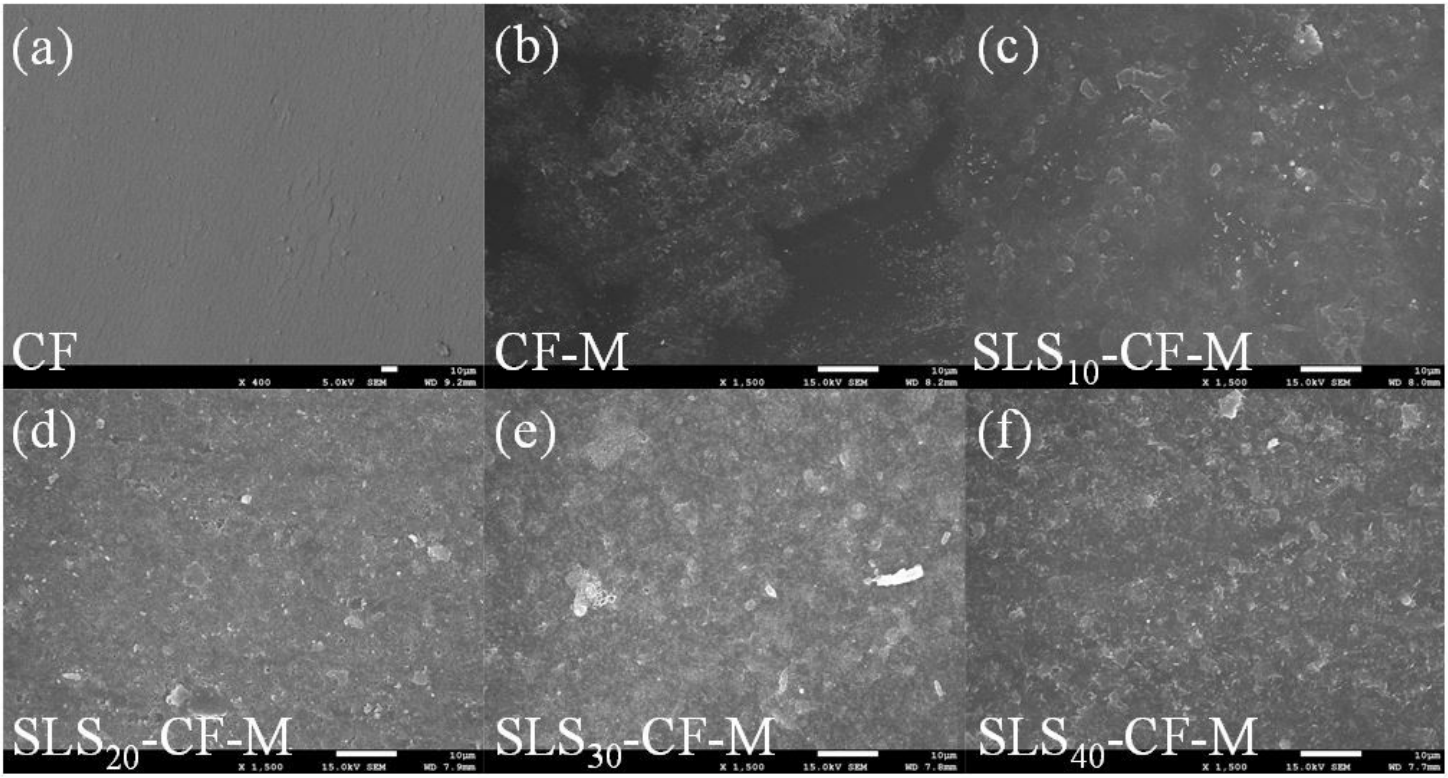

Figure 2

SEM images of pure CF (a), CF-M (b), and SLS10-40-CF-M (c-f).

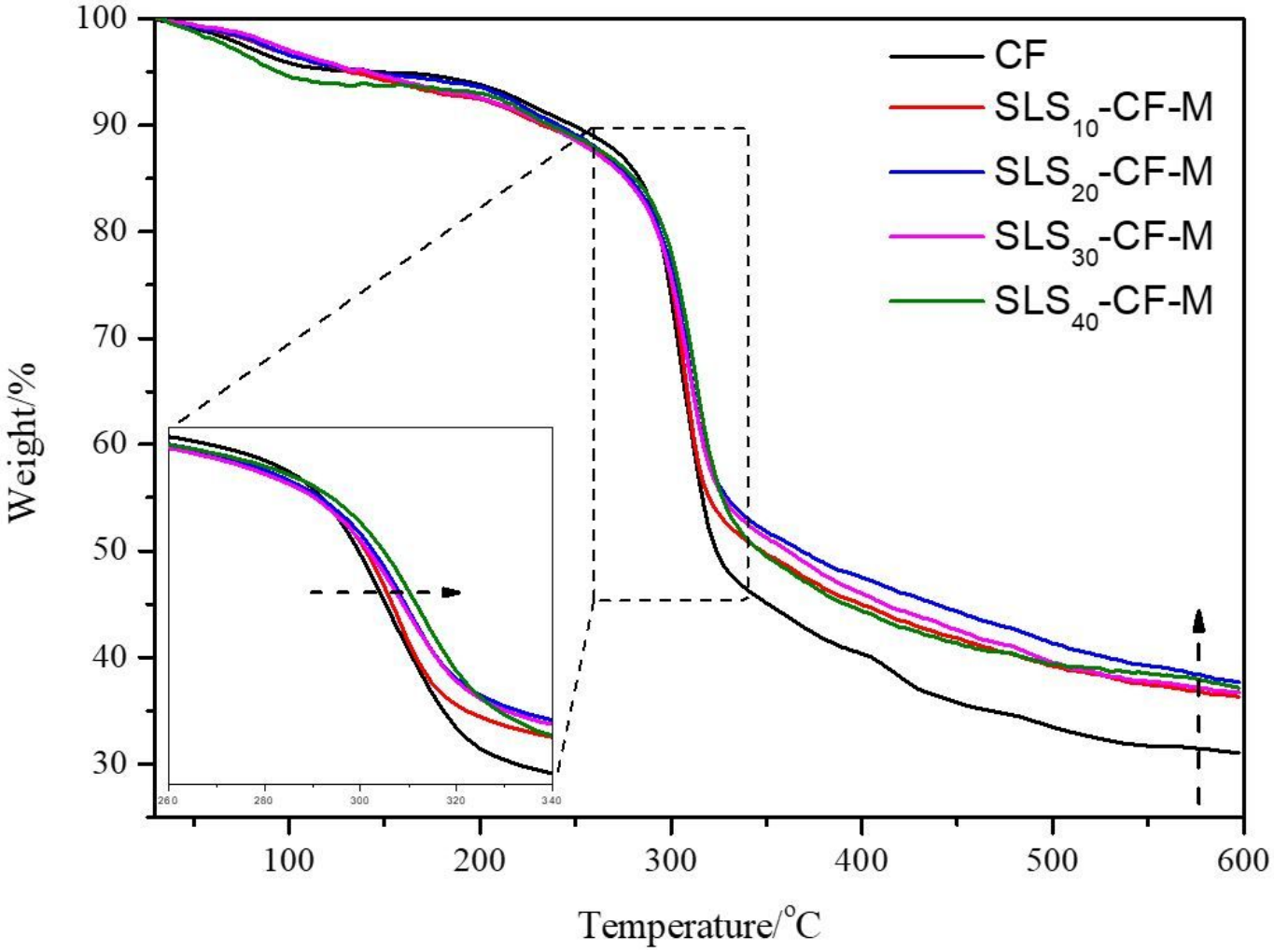

Figure 3

Thermal stability of pure CF and other modified blending films.

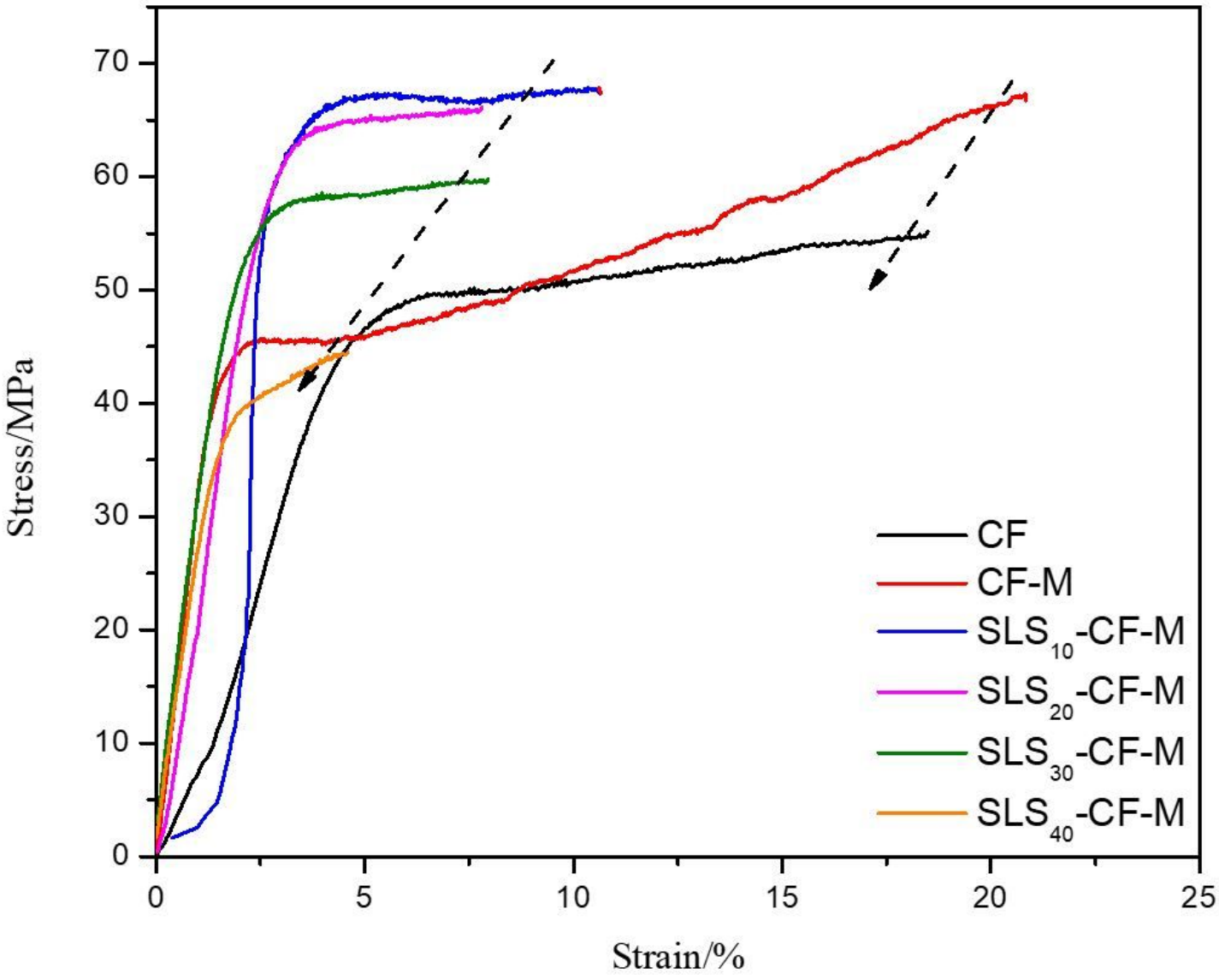

Figure 4

Stress-strain curves of pure CF, CF-M, and other modified blending films.

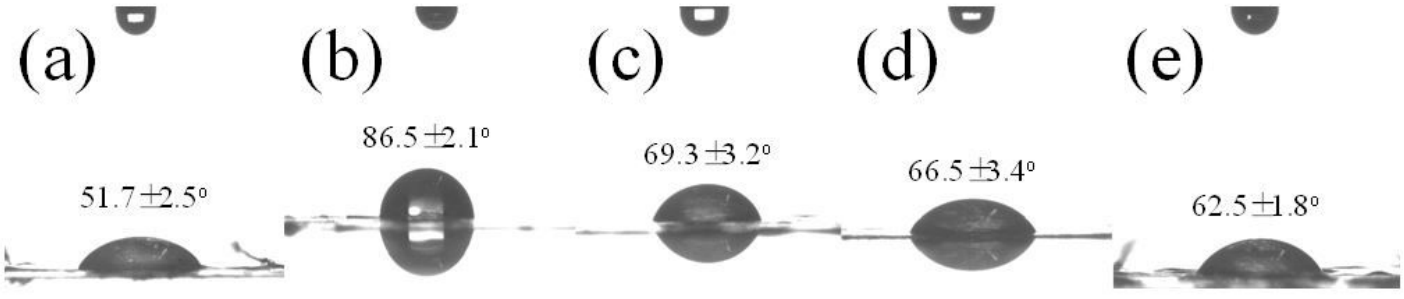

Figure 5

The contact angles of (a) pure CF, (b) SLS10-CF-M, (c) SLS20-CF-M, (d) SLS30-CF-M, and (e) SLS40-CF-M.

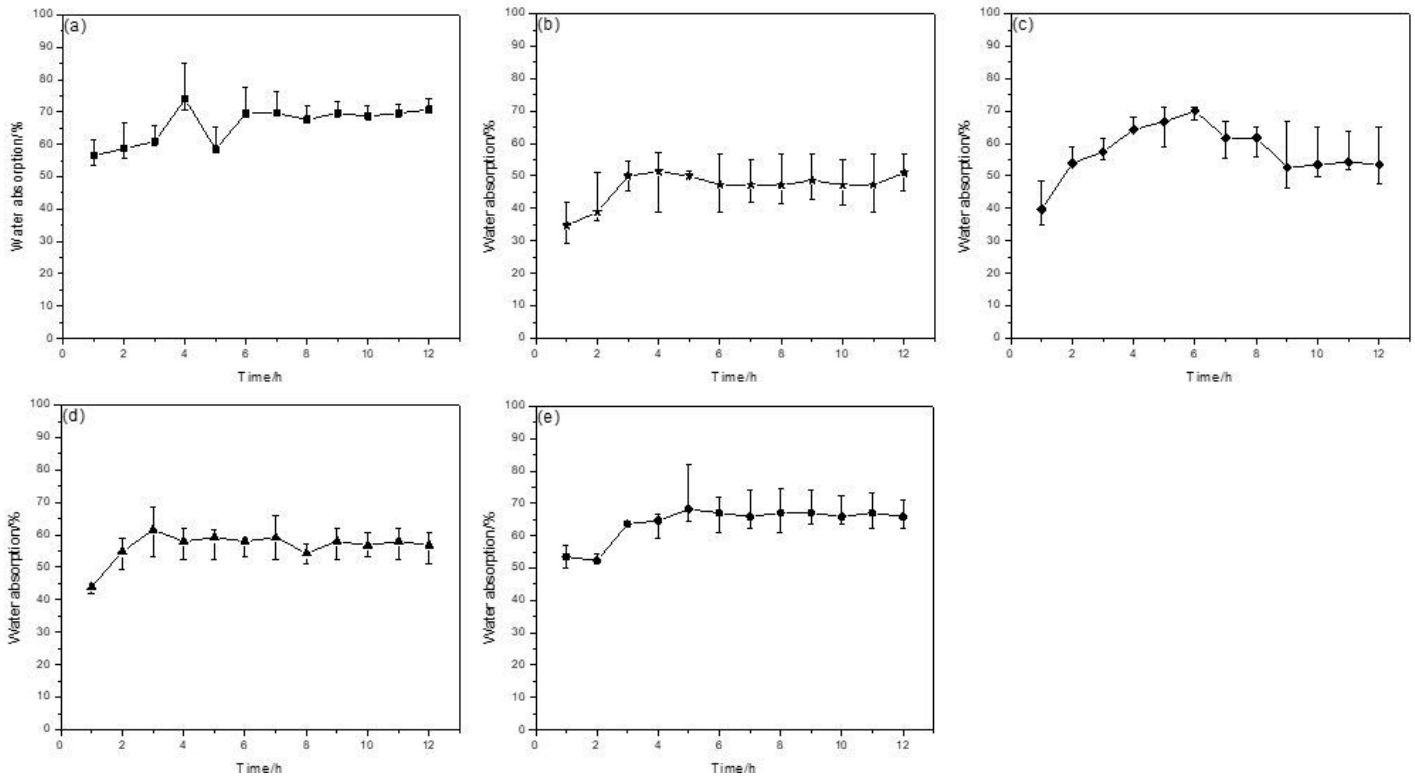

Figure 6

Water absorption capacity of pure CF (a) and modified blending films: (b) SLS10-CF-M, (c) SLS20-CF-M, (d) SLS30-CF-M, (e) SLS40-CF-M.

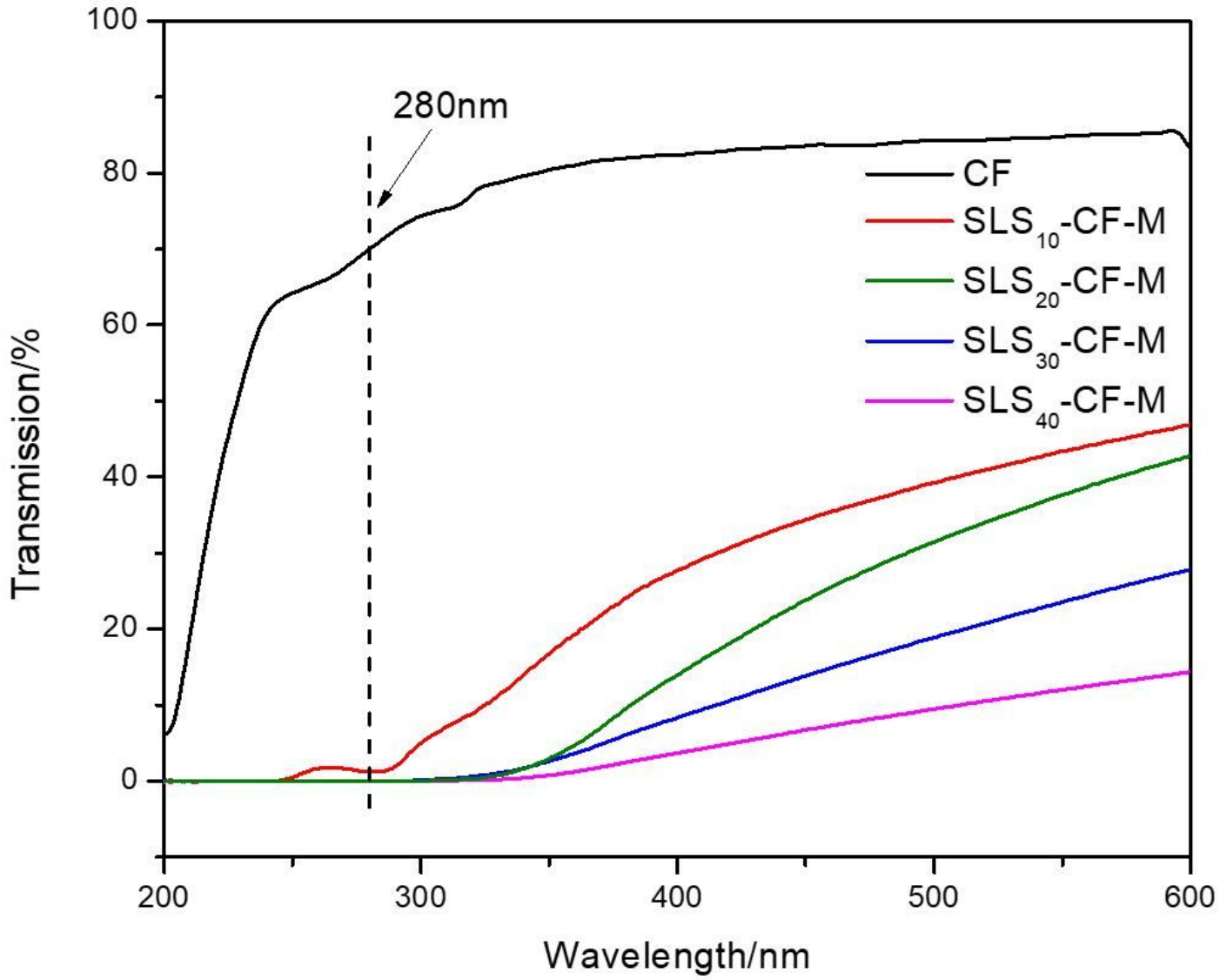

Figure 7

Visible-light transmittance curves of films.

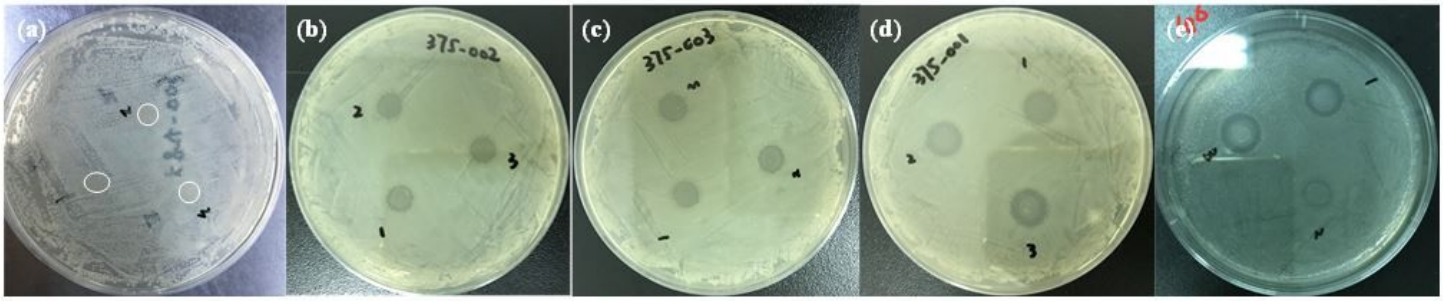

Figure 8

Antibacterial ability of (a) CF, (b) SLS10-CF-M, (c) SLS20-CF-M, (d) SLS30-CF-M, and (e) SLS40-CF-M.

Supplementary Files

This is a list of supplementary files associated with this preprint. Click to download.

- graphicsabstract.jpg
- scheme1.jpg